Comput. Methods Appl. Mech. Engrg. 198 (2009) 3278–3286

Contents lists available at ScienceDirect

Comput. Methods Appl. Mech. Engrg.

journal homepage: www.elsevier.com/locate/cma

Collision in a cross-shaped domain – A steady 2d Navier–Stokes example demonstrating the importance of mass conservation in CFD

Alexander Linke

Weierstrass Institute for Applied Analysis and Stochastics, Berlin, Germany

ARTICLE INFO

Article history:
Received 25 February 2009
Received in revised form 29 May 2009
Accepted 8 June 2009
Available online 30 June 2009

Keywords:
Incompressible Navier–Stokes equations
Mixed finite elements
Poor mass conservation
Numerical instability

ABSTRACT

In the numerical simulation of the incompressible Navier–Stokes equations different numerical instabilities can occur. While instability in the discrete velocity due to dominant convection and instability in the discrete pressure due to a vanishing discrete Ladyzhenskaya–Babuska–Brezzi (LBB) constant are well-known, instability in the discrete velocity due to a poor mass conservation at high Reynolds numbers sometimes seems to be underestimated. At least, when using conforming Galerkin mixed finite element methods like the Taylor–Hood element, the classical grad-div stabilization for enhancing discrete mass conservation is often neglected in practical computations. Though simple academic flow problems showing the importance of mass conservation are well-known, these examples differ from practically relevant ones, since specially designed force vectors are prescribed. Therefore, we present a simple steady Navier–Stokes problem in two space dimensions at Reynolds number 1024, a colliding flow in a cross-shaped domain, where the instability of poor mass conservation is studied in detail and where no force vector is prescribed.

1. Introduction

Classical finite element analysis for mixed approximations of the incompressible Navier–Stokes equation predicts that at high Reynolds numbers special care has to be taken, in order to prevent different numerical instabilities [26]. While instability due to dominant convection is well-known for a long time [23,17,8,26] and still remains an active area of research in the finite element community [14–16,3,5–7,11,21,22,18] instability due to poor mass conservation seems to be often underestimated [24,19]. But simple academic test examples with a purpose-built force vector (e.g., rotation-free) easily show that instability due to poor mass conservation can have dramatic consequences, even at moderate Reynolds numbers [28,24,11,19,9]. Nevertheless, stabilizing poor mass conservation by the classical grad-div stabilization is not very popular in practice, since the evolving linear systems become stiff and the convergence of iterative methods like multi-grid suffers due to this stabilization operator [24].

In this paper, we present a two-dimensional steady Navier–Stokes flow in a cross-shaped domain with two inflow and two outflow channels at Reynolds number 1024. The example illustrates, under which flow conditions poor mass conservation becomes a main problem in numerical Navier–Stokes computations. The example is non-academic in the sense that there is no artificially constructed right-hand side and the flow is driven only by reasonable velocity boundary conditions. For a numerical computation with mixed finite element methods the example poses two problems: first, a large curvature of the pressure develops, due to collision of the flow in the center of the cross-shaped domain. Second, boundary layers near corner singularities evolve, since the problem is singularly perturbed.

For this flow problem, we compare the approximation quality of the classical Galerkin Taylor–Hood element $(P_2 - P_1)$ [12,4], and the divergence-free Galerkin Scott–Vogelius element $(P_2 - P_{-1})$ [33,32,30,13,2,25,6,20,19]. In order to prevent instability due to dominant convection, we resolve the boundary layers by a customized anisotropic mesh. The chosen sequence of meshes also assures the Ladyzhenskaya–Babuska–Brezzi (LBB) stability of both mixed finite element methods [13,2,25]. Then the Galerkin Taylor–Hood element delivers numerical approximations that are spoiled by spurious oscillations due to poor mass conservation, while the divergence-free Galerkin Scott–Vogelius element yields stable and accurate numerical solutions [19]. The better accuracy of the Galerkin Scott–Vogelius method is numerically demonstrated by an investigation of the convergence behavior of both methods with respect to a reference solution. This superior behavior of the Scott–Vogelius element is remarkable, since the algebraic space of discretely divergence-free functions is much larger in the case of the Taylor–Hood element than in the case of the Scott–Vogelius element.

E-mail address: linke@wias-berlin.de

0045-7825/$ - see front matter © 2009 Elsevier B.V. All rights reserved.
doi:10.1016/j.cma.2009.06.016

2. The Stokes, Oseen and Navier–Stokes problems

We consider the following system of partial differential equations for $(\mathbf{u}, p)$ in a polygonal domain $\Omega \subset \mathbb{R}^2$.

$$\begin{aligned} &-\nu\Delta\mathbf{u} + (\mathbf{a}(\mathbf{u})\cdot\nabla)\mathbf{u} + \nabla p = \mathbf{f} \quad \text{in } \Omega,\\ &\nabla\cdot\mathbf{u} = 0 \quad \text{in } \Omega,\\ &\mathbf{u} = \mathbf{u}_D \quad \text{on } \Gamma_D,\\ &\mathbf{u}\cdot\mathbf{n} = 0, \quad \frac{\partial(\mathbf{u}\cdot\mathbf{t})}{\partial\mathbf{n}} = 0 \quad \text{on } \Gamma_S. \end{aligned} \tag{1}$$

The boundary $\partial\Omega$ is split in two different parts $\partial\Omega = \Gamma_D \cup \Gamma_S$ with $\Gamma_D \cap \Gamma_S$ being zero-dimensional. On Γ_D Dirichlet boundary conditions are prescribed, while on Γ_S symmetry boundary conditions apply. We assume that $\mathbf{u}_D \in [C(\Gamma_D)]^2$ is continuous and can be continued to a function $\mathbf{u}_B \in [H^1(\Omega)]^2$. The continuation can be constructed, e.g., by solving the following problem: find $\mathbf{u}_B \in \mathbf{A}$, with the affine trial space

$$\mathbf{A} := \{\mathbf{v} \in [H^1]^2 : \mathrm{trace}_{\Gamma_D}(\mathbf{v}) = \mathbf{u}_D \wedge \mathrm{trace}_{\Gamma_S}(\mathbf{v})\cdot\mathbf{n} = 0\}$$

and solve

$$(\nabla\mathbf{u}_B, \nabla\mathbf{v}) = 0$$

for all $\mathbf{v} \in \mathbf{V}$ with

$$\mathbf{V} := \{\mathbf{v} \in [H^1]^2 : \mathrm{trace}_{\Gamma_D}(\mathbf{v}) = \mathbf{0} \wedge \mathrm{trace}_{\Gamma_S}(\mathbf{v})\cdot\mathbf{n} = 0\}.$$

Here, $(\cdot,\cdot)$ denotes the L^2-scalar product. Further we assume that $\nu > 0$ is a constant and that $\mathbf{f} \in [L^2(\Omega)]^2$ holds.

For the convection term $(\mathbf{a}(\mathbf{u})\cdot\nabla)\mathbf{u}$ we will investigate three different choices

$$\mathbf{a}(\mathbf{u}) = \begin{cases} \mathbf{0}, & \text{the Stokes problem}\\ \mathbf{a}, & \text{the Oseen problem}\\ \mathbf{u}, & \text{the (nonlinear) Navier—Stokes problem.} \end{cases}$$

In the case of the Oseen problem, we assume that the conditions $\nabla\cdot\mathbf{a} = 0$ and $\mathbf{a}_{|\partial\Omega} = \mathbf{u}_{|\partial\Omega}$ hold and that $\mathbf{a}$ is as smooth as $\mathbf{u}$ is. Each of these equations describes the steady distribution of a velocity field $\mathbf{u}$ and a pressure field p in an incompressible fluid. The Stokes model is applied, when inertial forces are negligible and only frictional forces are important. The Navier–Stokes model is applied, when both frictional and inertial forces are relevant. The Oseen model has a rather limited physical meaning. It is a linearized Navier–Stokes problem and often serves as a model problem for a numerical analysis of the full Navier–Stokes problem.

For a weak formulation of problem (1), we introduce the Sobolev space

$$Q := L^2_0(\Omega) = \left\{ q \in L^2(\Omega) : \int_\Omega q(x)dx = 0 \right\}$$

and the new variable $\mathbf{u}_{\mathrm{hom}} := \mathbf{u} - \mathbf{u}_B$. Obviously, for $\mathbf{u}_{\mathrm{hom}}$ apply homogenous Dirichlet boundary conditions on Γ_D.

The weak formulation of this problem can be stated in the following saddle point form: find $(\mathbf{u}_{\mathrm{hom}}, p) \in \mathbf{V}\times Q =: \mathbf{X}$ such that

$$\begin{aligned} &a(\mathbf{u}_{\mathrm{hom}}, p, \mathbf{v}_{\mathrm{hom}}, q) + b(\mathbf{u}_{\mathrm{hom}}, p, \mathbf{v}_{\mathrm{hom}}, q) + b(\mathbf{v}_{\mathrm{hom}}, q, \mathbf{u}_{\mathrm{hom}}, p)\\ &\quad = l(\mathbf{v}_{\mathrm{hom}}, q) \end{aligned} \tag{2}$$

for all $(\mathbf{v}_{\mathrm{hom}}, q) \in \mathbf{X}$. Here, the forms $a(\cdot,\cdot) : \mathbf{X}\times\mathbf{X} \to \mathbb{R}, b(\cdot,\cdot) : \mathbf{X}\times\mathbf{X} \to \mathbb{R}$, and $l : \mathbf{X} \to \mathbb{R}$ are defined as

$$\begin{aligned} a(\mathbf{u}_{\mathrm{hom}}, p, \mathbf{v}_{\mathrm{hom}}, q) &:= \nu(\nabla\mathbf{u}_{\mathrm{hom}}, \nabla\mathbf{v}_{\mathrm{hom}}) \\ &\quad + ((\mathbf{a}(\mathbf{u}_B + \mathbf{u}_{\mathrm{hom}})\cdot\nabla)(\mathbf{u}_B + \mathbf{u}_{\mathrm{hom}}), \mathbf{v}_{\mathrm{hom}}), \end{aligned} \tag{3}$$

$$b(\mathbf{u}_{\mathrm{hom}}, p, \mathbf{v}_{\mathrm{hom}}, q) := -(\nabla\cdot\mathbf{u}_{\mathrm{hom}}, q), \tag{4}$$

$$\begin{aligned} l(\mathbf{v}_{\mathrm{hom}}, q) &:= (\mathbf{f}, \mathbf{v}_{\mathrm{hom}}) - \nu(\nabla\mathbf{u}_B, \nabla\mathbf{v}_{\mathrm{hom}}) + (\nabla\cdot\mathbf{u}_B, q) \end{aligned}$$

for all $(\mathbf{u}_{\mathrm{hom}}, p), (\mathbf{v}_{\mathrm{hom}}, q) \in \mathbf{X}$. The form $b(\cdot,\cdot)$ is bilinear and bounded, $l(\cdot)$ is linear and bounded, and $a(\cdot,\cdot)$ is linear in the second argument.

In the linear Stokes and Oseen cases the problem can be simplified further. In the Stokes problem the term $\mathbf{a}(\mathbf{u})$ drops out, and the form $a(\cdot,\cdot)$ is actually bilinear and bounded. In the Oseen case by moving one term to the right-hand side, we introduce the slightly modified forms

$$\begin{aligned} a_{\mathrm{Oseen}}(\mathbf{u}_{\mathrm{hom}}, p, \mathbf{v}_{\mathrm{hom}}, q) &:= \nu(\nabla\mathbf{u}_{\mathrm{hom}}, \nabla\mathbf{v}_{\mathrm{hom}}) + ((\mathbf{a}\cdot\nabla)\mathbf{u}_{\mathrm{hom}}, \mathbf{v}_{\mathrm{hom}}), \\ l_{\mathrm{Oseen}}(\mathbf{v}_{\mathrm{hom}}, q) &:= (\mathbf{f}, \mathbf{v}_{\mathrm{hom}}) - \nu(\nabla\mathbf{u}_B, \nabla\mathbf{v}_{\mathrm{hom}}) + (\nabla\cdot\mathbf{u}_B, q) \\ &\quad - ((\mathbf{a}\cdot\nabla)\mathbf{u}_B, \mathbf{v}_{\mathrm{hom}}) \end{aligned} \tag{5}$$

for all $(\mathbf{u}_{\mathrm{hom}}, p), (\mathbf{v}_{\mathrm{hom}}, q) \in \mathbf{X}$, and we must solve the problem: *find* $(\mathbf{u}_{\mathrm{hom}}, p) \in \mathbf{X}$ *such that*

$$\begin{aligned} &a_{\mathrm{Oseen}}(\mathbf{u}_{\mathrm{hom}}, p, \mathbf{v}_{\mathrm{hom}}, q) + b(\mathbf{u}_{\mathrm{hom}}, p, \mathbf{v}_{\mathrm{hom}}, q) + b(\mathbf{v}_{\mathrm{hom}}, q, \mathbf{u}_{\mathrm{hom}}, p)\\ &\quad = l_{\mathrm{Oseen}}(\mathbf{v}_{\mathrm{hom}}, q) \end{aligned} \tag{6}$$

holds for all $(\mathbf{v}_{\mathrm{hom}}, q) \in \mathbf{X}$. The form $a_{\mathrm{Oseen}}(\cdot,\cdot)$ is bilinear and bounded. Then an existence and uniqueness theory for the Stokes and Oseen problem is straight-forward. We define the space of divergence-free, weakly differentiable vector functions

$$\mathbf{V}_0 := \{\mathbf{v} \in \mathbf{V} : (\nabla\cdot\mathbf{v}, q) = 0 \quad \text{for all } q \in Q\}, \tag{7}$$

and the bilinear forms $a(\cdot,0,\cdot,0)$ and $a_{\mathrm{Oseen}}(\cdot,0,\cdot,0)$ restricted to the product space $\mathbf{V}_0\times\mathbf{V}_0$ are coercive, due to $\nabla\cdot\mathbf{a} = 0$. The existence of the pressure p is guaranteed by the Ladyzhenskaja condition, i.e., on the considered domain Ω it holds that for all $q \in Q$ there is a velocity $\mathbf{v} \in \mathbf{V}$ with $\nabla\cdot\mathbf{v} = q$ such that

$$\|\nabla\mathbf{v}\|_0 \leqslant C\|p\|_0,$$

with a constant C only depending on the shape of Ω, see [12].

The existence theory for the steady Navier–Stokes problem is more involved and needs the application of the theory of pseudomonotone operators, see Ref. [27]. Then uniqueness can be expected a priori only for large values of ν, i.e., $\nu = \mathcal{O}(1)$.

Below we will present a two-dimensional Navier–Stokes problem with $\mathbf{f} \equiv \mathbf{0}$, demonstrating the importance of mass conservation in numerical approximations of the Navier–Stokes equation. Then the flow is driven only by the inhomogeneous Dirichlet boundary conditions, and the rotation-free part of the convection term $(\mathbf{u}\cdot\nabla)\mathbf{u}$ arises as a source of a numerical instability. This numerical instability will be illustrated by theoretical considerations concerning an appropriate Stokes model problem with homogeneous Dirichlet boundary conditions and non-zero right-hand side $\mathbf{f}$.

3. Conforming Galerkin mixed finite elements

A conforming Galerkin mixed finite element discretization for the incompressible Stokes, Oseen or Navier–Stokes equations, starts directly from the weak formulation in Eq. (2). Applying this weak formulation, we choose finite-dimensional function spaces $\mathbf{V}^h \subset \mathbf{V}$ and $Q^h \subset Q$ serving as trial and test functions for the weak formulation in Eq. (2). Here, the term *Galerkin* means that we use the same function spaces for trial and test functions, while the term *conforming* emphasizes that the discrete spaces $\mathbf{V}^h$ and Q^h are really subspaces of $\mathbf{V}$ and Q. Since the mathematical nature of the quantities velocity and pressure in the incompressible Navier–Stokes equation are quite different, the term *mixed* is applied.

For the discretization of the incompressible Stokes, Oseen and Navier–Stokes equations, we use the classical Taylor–Hood element and the Scott–Vogelius element. Therefore, let $\overline{\mathscr{T}}^h$ denote a triangulation of the domain Ω without hanging nodes. For each triangle $\overline{T} \in \overline{\mathscr{T}}^h$, we define

$$h_{\overline{T}} := \max_{e \subset \partial \overline{T}} h_e,$$

with h_e the length of the edge e. Moreover, we assume that the mesh is regular in the following sense:

- (local shape regularity) for all simplices $\overline{T} \in \overline{\mathscr{T}}^h$

$$\frac{h_{\overline{T}}}{\operatorname{diam}(\overline{T})} < C$$

holds, where $\operatorname{diam}(\overline{T})$ means the diameter of the largest inscribed ball in $\overline{T}$ and C is a fixed constant;
- (local quasi uniformity) for any two elements $\overline{T}, \overline{T}' \in \overline{\mathscr{T}}^h$ having at least one common node $h_{\overline{T}} < \rho h_{\overline{T}'}$ holds, with a fixed constant $\rho > 0$.

Later on, the mesh $\overline{\mathscr{T}}^h$ is called a macro triangulation and we derive a second triangulation $\mathscr{T}^h$ from $\overline{\mathscr{T}}^h$. For each triangle $\overline{T} \in \overline{\mathscr{T}}^h$ we connect its barycenter with its vertices, and we thereby get three new triangles from each macro triangle. This new triangulation $\mathscr{T}^h$ is also locally shape regular and locally quasi uniform, although the constants for interpolation estimates are worse, because we get larger angles.

For the Taylor–Hood element and the Scott–Vogelius element we define $\mathbf{V}^h$ as the space of continuous elementwise quadratic vector functions on the triangulation $\mathscr{T}^h$

$$\mathbf{V}^h := \{\mathbf{v}^h \in [C(\Omega)]^2 : \mathbf{v}^h_{|T} \in P_2(T), \text{ for all } T \in \mathscr{T}^h\}.$$

Though these two mixed finite elements have the same discrete velocity space, they differ in the discrete pressure space. For the classical Taylor–Hood element we define

$$Q^h_{\mathrm{TH}} := \{q \in Q \cap C(\Omega) : q_{|T} \in P_1, \text{for all } T \in \mathscr{T}^h\},$$

while the pressure space of the Scott–Vogelius element is defined by

$$Q^h_{\mathrm{SV}} := \{q \in Q : q_{|T} \in P_1, \text{for all } T \in \mathscr{T}^h\}.$$

Therefore, the Taylor–Hood element and the Scott–Vogelius element have elementwise linear pressure functions, but for the latter the pressure functions are discontinuous. The above derivation of the triangulation $\mathscr{T}^h$ from a macro-triangulation $\overline{\mathscr{T}}^h$ assures that the Scott–Vogelius element is LBB stable on $\mathscr{T}^h$, see Refs. [25,2]. Also the LBB stability of the classical Taylor–Hood is assured on such triangulations, see Ref. [4].

The discretization of the problem in Eq. (2) is now given by: find $(\mathbf{u}^h_{\mathrm{hom}}, p^h) \in \mathbf{V}^h \times Q^h =: \mathbf{X}^h$ such that

$$a(\mathbf{u}^h_{\mathrm{hom}}, p^h, \mathbf{v}^h_{\mathrm{hom}}, q^h) + b(\mathbf{u}^h_{\mathrm{hom}}, p^h, \mathbf{v}^h_{\mathrm{hom}}, q^h) + b(\mathbf{v}^h_{\mathrm{hom}}, q^h, \mathbf{u}^h_{\mathrm{hom}}, p^h) = l(\mathbf{v}^h_{\mathrm{hom}}, q^h) \tag{8}$$

for all $(\mathbf{v}^h_{\mathrm{hom}}, q^h) \in \mathbf{X}^h$. Here, we have $\mathbf{X}^h = \mathbf{V}^h \times Q^h_{\mathrm{TH}}$ or $\mathbf{X}^h = \mathbf{V}^h \times Q^h_{\mathrm{SV}}$.

Similarly, we can discretize the Oseen problem in Eq. (6) as: find $(\mathbf{u}^h_{\mathrm{hom}}, p^h) \in \mathbf{X}^h$

$$a_{\mathrm{Oseen}}(\mathbf{u}^h_{\mathrm{hom}}, p^h, \mathbf{v}^h_{\mathrm{hom}}, q^h) + b(\mathbf{u}^h_{\mathrm{hom}}, p^h, \mathbf{v}^h_{\mathrm{hom}}, q^h) + b(\mathbf{v}^h_{\mathrm{hom}}, q^h, \mathbf{u}^h_{\mathrm{hom}}, p^h) = l_{\mathrm{Oseen}}(\mathbf{v}^h_{\mathrm{hom}}, q^h) \tag{9}$$

for all $(\mathbf{v}^h_{\mathrm{hom}}, q^h) \in \mathbf{X}^h$.

The Scott–Vogelius element is interesting for our investigation below, since its discrete velocity space and its discrete pressure space fulfill an important property, namely

$$\nabla \cdot \mathbf{V}^h \subset Q^h_{\mathrm{SV}}. \tag{10}$$

This property enforces exact mass conservation of the Scott–Vogelius element. Assuming that $\mathbf{u}_B \in \mathbf{V}^h$, we test Eq. (8) by $(\mathbf{0}, q^h)$ and obtain that

$$\begin{aligned} &-(\nabla \cdot \mathbf{u}^h_{\mathrm{hom}}, q^h) = (\nabla \cdot \mathbf{u}^B, q^h) \quad \Longleftrightarrow \\ &-(\nabla \cdot (\mathbf{u}^h_{\mathrm{hom}} + \mathbf{u}_B), q^h) = 0 \quad \Longleftrightarrow \\ &-(\nabla \cdot \mathbf{u}^h, q^h) = 0 \end{aligned} \tag{11}$$

holds for all $q^h \in Q^h_{\mathrm{SV}}$. Due to (10) we can choose the special test function $q^h := -\nabla \cdot \mathbf{u}^h$ and we have exact mass conservation in the L^2 sense. In general, the same pressure test function cannot be used in the Taylor–Hood case, since $\nabla \cdot \mathbf{V}^h \not\subset Q^h_{\mathrm{TH}}$. Hence the Taylor–Hood element only delivers discretely divergence-free approximations $\mathbf{u}^h$. A space of discretely divergence-free vector functions is then defined by

$$\mathbf{V}^h_0 = \{\mathbf{v}^h_{\mathrm{hom}} \in \mathbf{V}^h : (\mathbf{v}^h_{\mathrm{hom}}, q^h) = 0, \text{for all } q^h \in Q^h\}. \tag{12}$$

This space is crucially dependent on the pressure space Q^h. For $Q^h = Q^h_{\mathrm{SV}}$ we obtain $\mathbf{V}^h_0 \subset \mathbf{V}_0$, but for $Q^h = Q^h_{\mathrm{TH}}$ actually $\mathbf{V}^h_0 \not\subset \mathbf{V}_0$ holds.

In our investigation of mass conservation in mixed finite element discretizations, we therefore compare the discretely divergence-free Taylor–Hood element with the divergence-free Scott–Vogelius element. The assumption $\mathbf{u}_B \in \mathbf{V}^h$ will always be fulfilled in the numerical computations below.

4. FEM error estimates and instabilities for the Oseen problem

The Oseen problem in Eq. (6) will now serve as a model problem for the following discussions. For our subsequent considerations it is justified to restrict the presentation to the special case, when all Dirichlet boundary conditions are homogeneous, and there is a right-hand side $l(\cdot,\cdot) \neq 0$. Since we can assume $\mathbf{u}_B \equiv \mathbf{0}$, we have indeed $l_{\mathrm{Oseen}}(\mathbf{v}_{\mathrm{hom}}, q) = l_{\mathrm{Oseen}}(\mathbf{v}_{\mathrm{hom}})$ for all $\mathbf{v}_{\mathrm{hom}} \in \mathbf{V}$ and $q \in Q$, and $a_{\mathrm{Oseen}}(\mathbf{u}_{\mathrm{hom}}, p, \mathbf{v}_{\mathrm{hom}}, q) = a_{\mathrm{Oseen}}(\mathbf{u}_{\mathrm{hom}}, \mathbf{v}_{\mathrm{hom}})$ for all $\mathbf{u}_{\mathrm{hom}}, \mathbf{v}_{\mathrm{hom}} \in \mathbf{V}$ and $p, q \in Q$. We further abbreviate the bilinear form $b(\mathbf{u}^h_{\mathrm{hom}}, p^h, \mathbf{v}^h_{\mathrm{hom}}, q^h)$ by $b(\mathbf{u}^h_{\mathrm{hom}}, q^h) := -(\nabla \cdot \mathbf{u}_{\mathrm{hom}}, q)$. Due to $\nabla \cdot \mathbf{a} = 0$ the bilinear form $a_{\mathrm{Oseen}}(\cdot,\cdot)$ is coercive with coercivity constant ν. With $\mathbf{u}, \mathbf{v}, \mathbf{a} \in [H^1_0(\Omega)]^2$ its continuity constant can be estimated by

$$\begin{aligned} |a_{\mathrm{Oseen}}(\mathbf{u}, \mathbf{v})| &= |\nu(\nabla \mathbf{u}, \nabla \mathbf{v})| + |((\mathbf{a} \cdot \nabla)\mathbf{u}, \mathbf{v})| \\ &\leqslant \nu \|\nabla \mathbf{u}\|_0 \|\nabla \mathbf{v}\|_0 + \int_\Omega |\mathbf{a}||\nabla \mathbf{u}||\mathbf{v}| dx, \end{aligned}$$

with $|\cdot|$ denoting the Euclidean vector and matrix norms. It holds

$$\begin{aligned} \int_\Omega |\mathbf{a}||\nabla \mathbf{u}||\mathbf{v}| dx &\leqslant \left(\int_\Omega |\mathbf{a}|^4 dx\right)^{\frac{1}{4}} \left(\int_\Omega |\mathbf{v}|^4 dx\right)^{\frac{1}{4}} \left(\int_\Omega |\nabla \mathbf{u}|^2 dx\right)^{\frac{1}{2}} \\ &\leqslant c(\Omega) \|\nabla \mathbf{a}\|_0 \|\nabla \mathbf{u}\|_0 \|\nabla \mathbf{v}\|_0, \end{aligned}$$

according to Sobolev's embedding theorem with a constant $c(\Omega)$, see Refs. [1,27]. We arrive at

$$|a_{\mathrm{Oseen}}(\mathbf{u}, \mathbf{v})| \leqslant (\nu + c(\Omega)\|\nabla \mathbf{a}\|_0) \|\nabla \mathbf{u}\|_0 \|\nabla \mathbf{v}\|_0. \tag{13}$$

Because of $\mathbf{u}_B \equiv \mathbf{0}$, we have $\mathbf{u}^h = \mathbf{u}^h_{\mathrm{hom}} \in \mathbf{V}^h_0$. Testing Eq. (9) by $\mathbf{v}^h \in \mathbf{V}^h_0$, we obtain

$$a_{\mathrm{Oseen}}(\mathbf{u}^h, \mathbf{v}^h) = l_{\mathrm{Oseen}}(\mathbf{v}^h).$$

Here, the pressure being a Lagrangian parameter dropped out from the equation, since we are on the manifold $\mathbf{V}^h_0$. Now let $\mathbf{w}^h$ be an arbitrary element of $\mathbf{V}^h_0$. Then we introduce $\mathbf{v}^h := \mathbf{u}^h - \mathbf{w}^h \in \mathbf{V}^h_0$ and obtain

$$a_{\mathrm{Oseen}}(\mathbf{v}^h, \mathbf{v}^h) = l_{\mathrm{Oseen}}(\mathbf{v}^h) - a_{\mathrm{Oseen}}(\mathbf{w}^h, \mathbf{v}^h). \tag{14}$$

Since $\mathbf{v}^h \in \mathbf{V}^h$, we can take $\mathbf{v} = \mathbf{v}^h$ in Eq. (6) and get

$$a_{\text{Oseen}}(\mathbf{v}^h, \mathbf{v}^h) = a_{\text{Oseen}}(\mathbf{u} - \mathbf{w}^h, \mathbf{v}^h) + b(\mathbf{v}^h, p).$$

Moreover, since $\mathbf{v}^h \in \mathbf{V}_0^h$, we have $b(\mathbf{v}^h, q^h) = 0$ for all $q^h \in Q^h$. Hence

$$a_{\text{Oseen}}(\mathbf{v}^h, \mathbf{v}^h) = a_{\text{Oseen}}(\mathbf{u} - \mathbf{w}^h, \mathbf{v}^h) + b(\mathbf{v}^h, p - q^h) \tag{15}$$

holds for all $q^h \in Q^h$. Using the coercivity and continuity (13) of $a_{\text{Oseen}}(\cdot,\cdot)$, we obtain the estimate

$$\|\nabla \mathbf{v}^h\|_0 \leqslant \frac{1}{\nu}\left((\nu + c(\Omega)\|\nabla \mathbf{a}\|_0)\|\nabla \mathbf{u} - \nabla \mathbf{w}^h\|_0 + \inf_{q^h \in Q^h} \sup_{\mathbf{0} \neq \mathbf{v}^h \in \mathbf{V}_0^h} \frac{(\nabla \cdot \mathbf{v}^h, p - q^h)}{\|\nabla \mathbf{v}^h\|_0} \right). \tag{16}$$

With the triangle inequality

$$\|\nabla \mathbf{u} - \nabla \mathbf{u}^h\|_0 \leqslant \|\nabla \mathbf{u} - \nabla \mathbf{w}^h\|_0 + \|\nabla \mathbf{v}^h\|_0$$

and Eq. (16) we finally arrive at

$$\|\nabla \mathbf{u} - \nabla \mathbf{u}^h\|_0 \leqslant \left(2 + \frac{c(\Omega)\|\nabla \mathbf{a}\|_0}{\nu}\right) \inf_{\mathbf{w}^h \in \mathbf{V}_0^h} \|\nabla \mathbf{u} - \nabla \mathbf{w}^h\|_0 + \frac{1}{\nu} \inf_{q^h \in Q^h} \sup_{\mathbf{0} \neq \mathbf{v}^h \in \mathbf{V}_0^h} \frac{(\nabla \cdot \mathbf{v}^h, p - q^h)}{\|\nabla \mathbf{v}^h\|_0}. \tag{17}$$

Remark 1. Note that the term

$$\frac{1}{\nu} \inf_{q^h \in Q^h} \sup_{\mathbf{0} \neq \mathbf{v}^h \in \mathbf{V}_0^h} \frac{(\nabla \cdot \mathbf{v}^h, p - q^h)}{\|\nabla \mathbf{v}^h\|_0} \tag{18}$$

vanishes for the Scott–Vogelius element, since then $\mathbf{V}_0^h \subset \mathbf{V}_0$ holds. Therefore, this term reflects a numerical instability of mixed Galerkin finite element discretizations, when discrete mass-conservation is not guaranteed well. This numerical instability can be controlled by using additional stabilization operators in the discrete variational formulation, like the grad-div stabilization [24,26].

Remark 2. For $p \in H^2(\Omega)$ using the Taylor–Hood element, the term (18) can be estimated by

$$\frac{1}{\nu} C|p|_2 h^2, \tag{19}$$

due to $\|\nabla \cdot \mathbf{v}\|_0 \leqslant \|\nabla \mathbf{v}\|_0$ for all $\mathbf{v} \in \mathbf{V}$, the properties of the L^2-projection for the pressure and the elementwise linear pressure trial functions of the Taylor–Hood element. Here, the constant C depends on the chosen mesh sequence $\mathscr{T}^h$. This estimate shows that problems with mass conservation appear for the Taylor–Hood element, when the curvature of the continuous pressure p is large.

Remark 3. In many flow problems a stabilization of mass conservation is not necessary. For instance, in a Hagen–Poiseuille channel flow, the continuous pressure p is proportional to ν. Then the amplification by $\frac{1}{\nu}$ in the error term (18) drops out, and the effect is negligible.

4.1. A numerical illustration of the Oseen error estimate

The error estimate in Inequality (17) predicts that large errors in the velocity approximation can occur, when the continuous pressure p is not part of the discrete pressure space Q^h, because violations of discrete mass conservation are amplified by the factor $\frac{1}{\nu}$ within the error term (18). For small viscosities of ν this amplification can be arbitrarily large. The question remains, whether the estimate (17) is sharp. In order to answer this question positively, we construct a simple, but illustrative example.

In the example, we investigate the Stokes problem with $\nu \in \{1, 10^{-4}\}$, and $\mathbf{a}(\mathbf{u}) \equiv \mathbf{0}$. We approximate the following test problem on $\Omega = [0,1]^2$ with the force vector $\mathbf{f} = c(3x^2 + 1, 3y^2)^T$ with $c \in \{1, 10, 100\}$ a constant parameter. On the boundary we prescribe homogeneous Dirichlet boundary conditions. Then the continuous solution of the Stokes problem is

$$(\mathbf{u}, p) = (\mathbf{0}, c(x^3 + y^3 + x - 1)). \tag{20}$$

We call this problem the "no flow example". First, this problem will be approximated with the Scott–Vogelius and the Taylor–Hood elements on the first refinement of the left grid in Fig. 1. Since this grid is derived from a macro-element grid, the Scott–Vogelius and the Taylor–Hood elements are LBB stable on it. In the Tables 1 and 2 we present some error norms for the approximation of the "no flow example" by the Galerkin Scott–Vogelius and the Galerkin Taylor–Hood elements. In Table 3 we demonstrate that a considerable improvement of the Galerkin Taylor–Hood results in Table 2 is possible by adding the grad-div stabilization[24,26] into the momentum balance, i.e., adding the term $-\gamma \nabla \nabla \cdot \mathbf{u}$ with a stabilization parameter γ. In the numerical test we set $\gamma = 1$. In the Galerkin Taylor–Hood discretization (Table 2), the numerical results for the error in the velocity approximation are proportional to $\frac{c}{\nu}$, while the pressure error scales only with c. The Scott–Vogelius element (Table 1) has the same dependence on c for the pressure error, but always delivers exact velocity approximations, since the continuous velocity $\mathbf{0}$ lies in the approximation space $\mathbf{V}^h$ and the error term (18) is zero for the Scott–Vogelius element. From error estimate (17) we recognize that the quality of Scott–Vogelius approximations for the velocity is completely independent of the continuous pressure. The velocity error for the Taylor–Hood element with grad-div stabilization $\gamma = 1$ (Table 3) is proportional to the constant c, but it is rather independent of ν. Further we recognize from Table 4 that it would be not fair, to judge the Galerkin Taylor–Hood element according to the results from Table 2. In the Taylor–Hood case, grids according to the construction principle of the left grid in Fig. 1 can be replaced by grids with better angle conditions, see, e.g., the right grid in Fig. 1. Table 4 demonstrates that the velocity error of the unstabilized Galerkin Taylor–Hood element can be reduced by a factor 10 using a better mesh than in Table 2. Nevertheless the dependence of the velocity error on $\frac{c}{\nu}$ remains. In the Scott–Vogelius case we use grids of the left type, since we want to assure LBB stability.

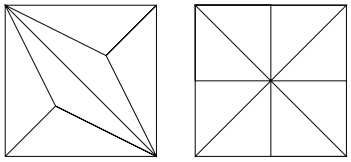

Fig. 1. The two basic meshes for the domain $\Omega = [0,1]^2$ used for checking the sharpness of the error estimate (17). Refined meshes consist of 4, 16, 64,... copies of these basic meshes.

Table 1
Error norms for a Scott–Vogelius discretization of the "no flow example" on the first refinement of the left grid in Fig. 1.

ν	c	$\|\nabla \mathbf{u} - \nabla \mathbf{u}^h\|_{0,\Omega}$	$\|\mathbf{u} - \mathbf{u}^h\|_{0,\Omega}$	$\|p - p^h\|_0$
1	1	0	0	6.27×10^{-1}
1	10	0	0	$6.27 \times 10^{+0}$
1	100	0	0	$6.27 \times 10^{+1}$
10^{-4}	1	0	0	6.27×10^{-1}
10^{-4}	10	0	0	$6.27 \times 10^{+0}$
10^{-4}	100	0	0	$6.27 \times 10^{+1}$

Table 2
Error norms for a Taylor–Hood discretization (without grad-div stabilization) of the "no flow example" on the first refinement of the left grid in Fig. 1.

ν	c	$\|\nabla\mathbf{u}-\nabla\mathbf{u}^h\|_{0,\Omega}$	$\|\mathbf{u}-\mathbf{u}^h\|_{0,\Omega}$	$\|p-p^h\|_0$
1	1	2.09×10^{-2}	1.41×10^{-3}	6.27×10^{-1}
1	10	2.09×10^{-1}	1.41×10^{-2}	$6.27\times10^{+0}$
1	100	$2.09\times10^{+0}$	1.41×10^{-1}	$6.27\times10^{+1}$
10^{-4}	1	$2.09\times10^{+2}$	$1.41\times10^{+1}$	6.27×10^{-1}
10^{-4}	10	$2.09\times10^{+3}$	$1.41\times10^{+2}$	$6.27\times10^{+0}$
10^{-4}	100	$2.09\times10^{+4}$	$1.41\times10^{+3}$	$6.27\times10^{+1}$

Table 3
Error norms for a Taylor–Hood discretization with grad-div stabilization $\gamma=1$ of the "no flow example" on the first refinement of the left grid in Fig. 1.

ν	c	$\|\nabla\mathbf{u}-\nabla\mathbf{u}^h\|_{0,\Omega}$	$\|\mathbf{u}-\mathbf{u}^h\|_{0,\Omega}$	$\|p-p^h\|_0$
1	1	1.20×10^{-2}	8.32×10^{-4}	6.30×10^{-1}
1	10	1.20×10^{-1}	8.32×10^{-3}	$6.30\times10^{+0}$
1	100	$1.20\times10^{+0}$	8.32×10^{-2}	$6.30\times10^{+1}$
10^{-4}	1	3.97×10^{-2}	2.78×10^{-3}	6.27×10^{-1}
10^{-4}	10	3.97×10^{-1}	2.78×10^{-2}	$6.27\times10^{+0}$
10^{-4}	100	$3.97\times10^{+0}$	2.78×10^{-1}	$6.27\times10^{+1}$

Table 4
Error norms for a Taylor–Hood discretization (without grad-div stabilization) of the "no flow example" on the first refinement of the right grid in Fig. 1.

ν	c	$\|\nabla\mathbf{u}-\nabla\mathbf{u}^h\|_{0,\Omega}$	$\|\mathbf{u}-\mathbf{u}^h\|_{0,\Omega}$	$\|p-p^h\|_0$
1	1	2.39×10^{-3}	1.04×10^{-4}	6.28×10^{-1}
1	10	2.39×10^{-2}	1.04×10^{-3}	$6.28\times10^{+0}$
1	100	2.39×10^{-1}	1.04×10^{-2}	$6.28\times10^{+1}$
10^{-4}	1	$2.39\times10^{+1}$	$1.04\times10^{+0}$	6.28×10^{-1}
10^{-4}	10	$2.39\times10^{+2}$	$1.04\times10^{+1}$	$6.28\times10^{+0}$
10^{-4}	100	$2.39\times10^{+3}$	$1.04\times10^{+2}$	$6.28\times10^{+1}$

The problem of the Taylor–Hood element with approximating the "no flow example" is due to the special right-hand side $\mathbf{f}=c(3x^2+1,3y^2)^T$. This right-hand side is rotation-free. In the Scott–Vogelius case, the corresponding linear form

$$l(\mathbf{v}^h)=\int_\Omega \mathbf{f}\cdot\mathbf{v}^h\,dx$$

is zero for all $\mathbf{v}^h\in\mathbf{V}_0^h$, since rotation-free vector functions are orthogonal to divergence-free vector functions in the L^2 scalar product. The numerical instability of the Taylor–Hood element arises, since here the discrete space $\mathbf{V}_0^h$ is not perpendicular to the rotation-free vector functions. This numerical instability is visible by *spurious oscillations* in the Taylor–Hood approximation of the "no flow example", see Fig. 2. In Fig. 2 the graph of the pressure p is presented.

5. Collision in a cross-shaped domain

In this Section, we present and describe a flow problem for the stationary 2D Navier–Stokes equations, where the Galerkin Scott–Vogelius discretization delivers better numerical approximations than the Galerkin Taylor–Hood discretization. The presented example is simple and possesses physical relevance. Moreover, this flow problem is especially interesting, since we prescribe a zero force vector $\mathbf{f}=\mathbf{0}$. In this case, numerical instabilities in the Galerkin Taylor–Hood method due to a weak mass conservation have their origin in the curvature of the pressure p polluting the velocity approximations, see the error term (19). According to this estimate, the effect should be visible at high Reynolds numbers, due to the amplification factor $\frac{1}{\nu}$.

We want to emphasize that it is not our goal to claim that the Scott–Vogelius element is in any way better for numerical computations than the Taylor–Hood element. Indeed, the numerical results for the Taylor–Hood element could be easily improved, either by using the grad-div stabilization or by using more appropriate meshes, see Section 4.1. We rather focus on the flow example itself and want to demonstrate, under which conditions mass conservation is important in practical numerical computations.

The idea for the construction of the example is as follows: we write the momentum equation of the steady Navier–Stokes equations in the form

$$-\nu\Delta\mathbf{u}+\nabla p=-(\mathbf{u}\cdot\nabla)\mathbf{u}.$$

Wherever in Ω the friction forces $-\nu\Delta\mathbf{u}$ are negligible, the convection term $(\mathbf{u}\cdot\nabla)\mathbf{u}$ must have a big rotation-free part due to $\nabla p\approx-(\mathbf{u}\cdot\nabla)\mathbf{u}$. Then a numerical approximation with the Galerkin Taylor–Hood element should suffer from spurious oscillations due

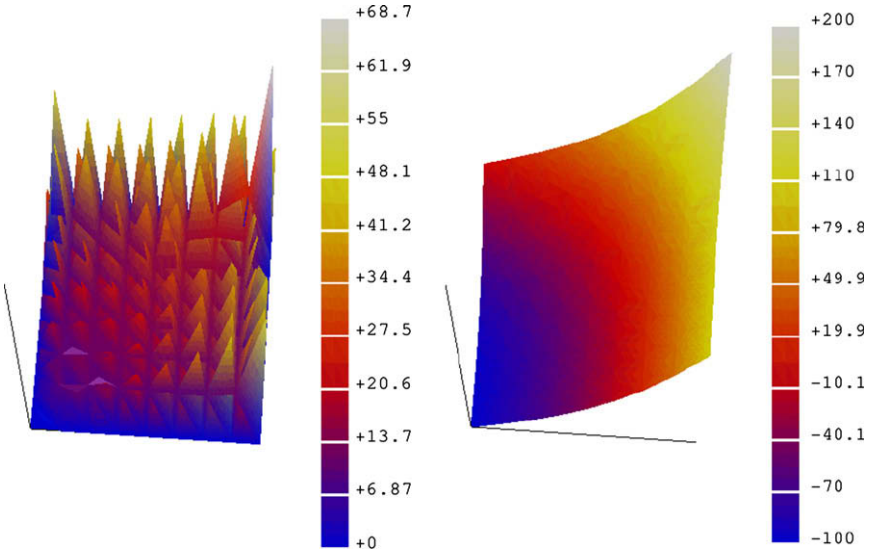

Fig. 2. No-flow example with $\nu=1.0\times10^{-4}$, and $c=100$: Left picture: graph of the absolute values $|\mathbf{u}^h|$ for a discrete Galerkin Taylor–Hood solution on the third refinement of the left mesh shown in Fig. 1. Right picture: graph of the corresponding pressure p^h.

to weak mass conservation, just as in the case with the above "no flow example". There the rotation-free force vector $\mathbf{f}$ causes problems, and in the example below the rotation-free part of $-(\mathbf{u}^h \cdot \nabla)\mathbf{u}^h$ will be the trouble-maker.

The example consists of a colliding flow in a cross-shaped domain

$$\Omega_{\text{phys}} = [-32, 33] \times [0, 1] \cup [0, 1] \times [-32, 33]$$

with Hagen–Poiseuille inflow boundary conditions in the north and the south of the domain, and Hagen–Poiseuille outflow boundary conditions in the west and in the east of the domain, see Fig. 3. The maximum velocities of the four Hagen–Poiseuille profiles are set to one. We define the Reynolds number of the flow by the Reynolds number at the inflow, analogous to Hagen–Poiseuille flows, namely

$$\text{Re} := \frac{1}{\nu}.$$

It turns out that for the considered small Reynolds numbers $\text{Re} \leqslant 1024$, the computed discrete Navier–Stokes approximations are steady, unique and symmetric along the north-south and the west-east axes, see Fig. 8.

Therefore, a completely symmetric setting was used for the actual computations below, restricting the flow problem to one quarter of the entire domain by using symmetry boundary conditions. The (computational) domain used is also shown in Fig. 3 and is described as

$$\Omega = [-32, 0] \times \left[0, \frac{1}{2}\right] \cup \left[0, \frac{1}{2}\right] \times [-32, 0] \cup \left[0, \frac{1}{2}\right] \times \left[0, \frac{1}{2}\right].$$

Different boundary conditions were prescribed on different parts of the domain:

$$\Gamma_0 := \{0\} \times [-32, 0] \cup [-32, 0] \times \{0\},$$
$$\Gamma_1 := \left[0, \frac{1}{2}\right] \times \{-32\},$$
$$\Gamma_2 := \{-32\} \times \left[0, \frac{1}{2}\right],$$
$$\Gamma_3 := \left\{\frac{1}{2}\right\} \times \left[-32, \frac{1}{2}\right] \cup \left[-32, \frac{1}{2}\right] \times \left\{\frac{1}{2}\right\}.$$

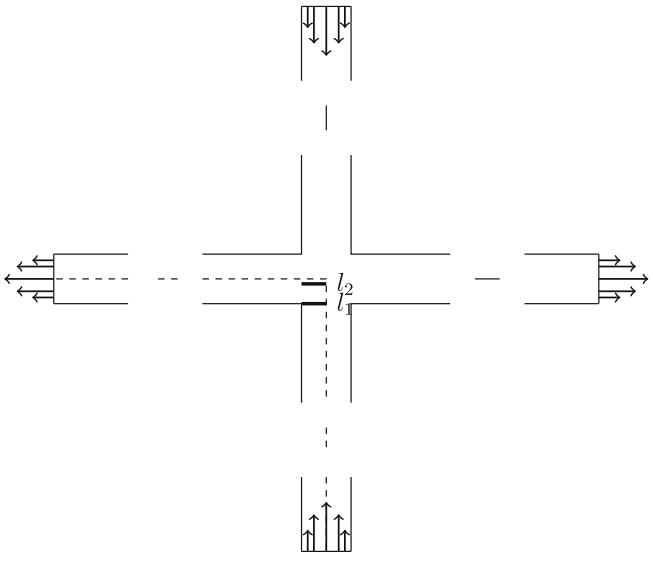

Fig. 3. Details from the physical and the computational domains, where the colliding flow problem is posed. The continuous lines denote the entire cross-shaped physical domain. The continuous and the dashed lines in the south-west quarter of the physical domain denote the actual computational domain. The dashed lines denote the symmetry boundary Γ_S. On the two thick lines l_1 and l_2 the horizontal and the vertical velocities are investigated below.

The partition into Dirichlet and symmetry boundary conditions is given by

$$\Gamma_D = \Gamma_0 \cup \Gamma_1 \cup \Gamma_2,$$
$$\Gamma_S = \Gamma_3.$$

We prescribe homogeneous Dirichlet boundary conditions at Γ_0. Here it is possible that boundary layers evolve. At the boundary Γ_1 we prescribe an inflow Dirichlet boundary condition with a Hagen–Poiseuille profile. At the boundary Γ_2, we prescribe an outflow Dirichlet boundary condition, also with a Hagen–Poiseuille profile:

$$\mathbf{u}(x, y) = (0, 4x(1 - x)) \quad \text{for all } \mathbf{x} \in \Gamma_1,$$
$$\mathbf{u}(x, y) = (-4y(1 - y), 0) \quad \text{for all } \mathbf{x} \in \Gamma_2.$$

In both cases, we only prescribe one half of the Hagen–Poiseuille profile, since we use symmetry boundary conditions at the boundary Γ_S. The symmetry boundary condition $\mathbf{u} \cdot \mathbf{n} = 0$ was imposed strongly, while the boundary condition $\partial(\mathbf{u} \cdot \mathbf{t})/\partial\mathbf{n} = \mathbf{0}$ is prescribed weakly.

We remark that a Navier–Stokes solution on the domain Ω can be extended to a Navier–Stokes solution on Ω_{phys} by reflecting the solution at the axes $x = \frac{1}{2}$ and $y = \frac{1}{2}$.

The most interesting part of the solution $(\mathbf{u}, p)$ is, where the collision of the flow actually happens, namely

$$\Omega_{\text{collision}} = \left[0, \frac{1}{2}\right] \times \left[0, \frac{1}{2}\right].$$

The rest of the domain $\Omega \setminus \Omega_{\text{collision}}$, i.e., the long channels coming from the inlet and conducting to the outlet, only serve to set up more or less realistic inflow and outflow boundary conditions.

Solving this colliding flow problem for Reynolds numbers $Re < 100$, allows us to see a typical behavior of the continuous pressure. The L^2 norm of the pressure seems to be proportional to ν. This is well-known from channel flows. The effect of the term (18) in Galerkin Taylor–Hood computations is then small, since the amplifying factor $\frac{1}{\nu}$ is multiplied by ν canceling each other out. But for Reynolds numbers larger than 100 the L^2 norm of the pressure increases slowly with the Reynolds number, and we expect to observe spurious divergence oscillations. The reason for this is that the pressure gradient has to balance the inertial forces, since the flow runs around a corner.

In the next section, we will present numerical results for this flow problem at the moderate Reynolds number 1024. Obviously, one would expect to observe the effect the better, the coarser the underlying mesh is. But then one must pay attention to another problem. Oscillations on coarse meshes at high Reynolds number arise due to two different reasons, mass conservation mirrored by the term (18), and dominance of convection due to non-resolved boundary layers. This leads to an interesting observation. When one compares the approximation quality of the Galerkin Taylor–Hood element and the Galerkin Scott–Vogelius element, the Taylor–Hood method is usually superior, when we use uniform triangulations of the domain. The reason is that the Scott–Vogelius element has much fewer discretely divergence-free trial functions than the Taylor–Hood element, since its discrete pressure space is discontinuous. Therefore, the Taylor–Hood element has more trial functions for approximating boundary layers, and this usually outweighs its disadvantage with respect to its non-zero divergence. But the situation is completely different on meshes where all boundary layers are adequately resolved by the mesh. Therefore, we use meshes for the following computations, which are refined in an anisotropic way at the boundary Γ_0. Additionally, at the corner (0, 0), we use an isotropic mesh refinement. In Fig. 4 we see a typical macro element grid, used for our computations. After constructing the real computation grid by adding the barycenters of all macro triangles, the Taylor–Hood and the Scott–Vogelius

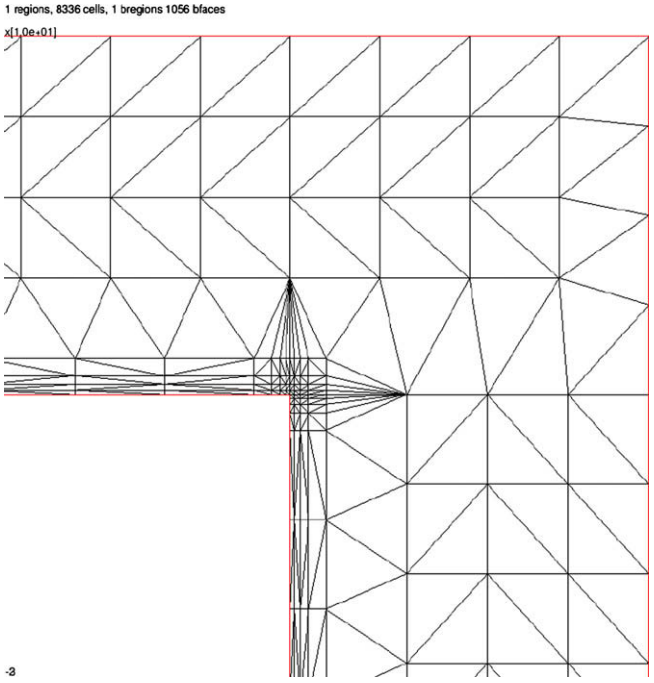

Fig. 4. Detail from the center of a macro element triangulation used for the colliding flow example. Note the anisotropic triangulation at the Dirichlet boundary Γ_0 and the isotropic triangulation around the corner (0, 0).

approximations are LBB stable on such grids, see Refs. [25,2]. For the construction of the grids, we use an estimated width of the boundary layer of about 0.05. We resolve the boundary layer with the same number of points as the coarser region in the interior of the domain, and we generated grids with 2, 4, 8, 16 and 32 points in the boundary layer. For the grid generation we used the mesh generator TRIANGLE [31].

6. Numerical results

In this section, we compare the numerical results obtained with the Galerkin Scott–Vogelius and the Galerkin Taylor–Hood method on the grids described in the previous section. All these computations have been performed with the finite element toolbox ALBERTA [29]. Some information on the Galerkin Scott–Vogelius and the Galerkin Taylor–Hood discretizations on these grids is shown in Tables 5 and 6. We clearly observe that the space $\mathbf{V}_0^h$ corresponding to the Taylor–Hood method is much larger than the respective space for the Scott–Vogelius element.

First, we show the global convergence behavior of the L^2 norm in the entire domain Ω in Fig. 5. From this Figure we conclude that the velocity L^2 norm for the Scott–Vogelius element converges significantly faster than the corresponding L^2 norm for the Taylor–Hood element. Unfortunately, we could not draw such clear conclusions for the H^1 norm of the velocities and the L^2 norm of the

Table 5
Colliding flow (with symmetry assumption): degrees of freedom (DOF) for the Galerkin Scott–Vogelius element.

Level	1	2	3	4	5
Velocity DOF	26,114	102,146	403,970	1,606,658	6,408,194
Pressure DOF	18,792	75,024	299,808	1,198,656	4,793,472
Div-free DOF	7,322	27122	104,162	408,002	1,614,722
Total DOF	44,906	177,170	703,778	2,805,314	11,201,666
Div-free/total	0.16	0.15	0.15	0.15	0.14

Table 6
Colliding flow (with symmetry assumption): degrees of freedom for the Galerkin Taylor–Hood element. Div-free stands for discretely divergence-free.

Level	1	2	3	4	5
Velocity DOF	26,114	102,146	403,970	1,606,658	6,408,194
Pressure DOF	3,397	13,033	51,025	201,889	803,137
Div-free DOF	22,717	89,113	352,945	1,404,769	5,605,057
Total DOF	29,511	115,179	454,995	1,808,547	7,211,331
Div-free/total	0.77	0.77	0.78	0.78	0.78

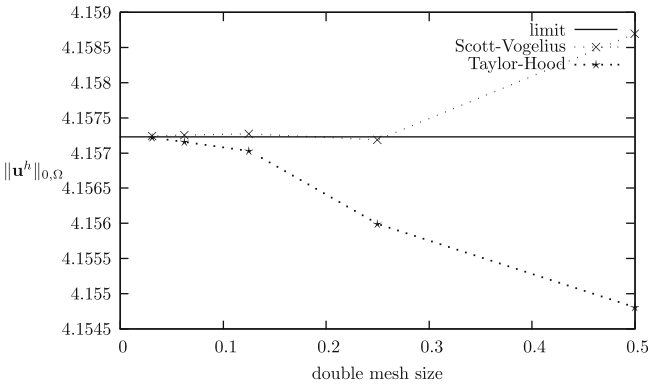

Fig. 5. Colliding flow in a cross-shaped domain (with symmetry assumption): convergence behavior of $\|\mathbf{u}^h\|_{0,\Omega}$ for Galerkin Scott–Vogelius and Galerkin Taylor–Hood discretizations. x-axis: $2.0 \times$ mesh size. y-axis: $\|\mathbf{u}^h\|_{0,\Omega}$. The abbreviation limit stands for an interpolated limit of $\|\mathbf{u}^h\|_{0,\Omega}$ for $h \to 0$.

pressure. Here, neither element type showed a definite asymptotic convergence behavior, and so we were not able to decide whether one element was superior than the other.

Since better convergence of $\|\mathbf{u}^h\|_{0,\Omega}$ to $\|\mathbf{u}\|_{0,\Omega}$ does not necessarily tell us that $\mathbf{u}^h$ also converges to $\mathbf{u}$ faster, we tried to compute a reference solution on a quite fine grid, in order to compare the convergence of Taylor–Hood and Scott–Vogelius approximations against this reference solution. The largest linear systems the direct solver PARDISO [10] could solve, had 11, 201, 666 degrees of freedom. At the next refinement step, the direct solver had insufficient memory available on our computer.

Since we are mainly interested in the flow field within $\Omega_{\text{collision}}$, we implemented a discrete L^2 norm for evaluating the difference between two approximations $\mathbf{u}^h$ and $\tilde{\mathbf{u}}^h$ at 961 points within $\Omega_{\text{collision}}$. In the following, this discrete norm will be called $l^2_{961}(.,.)$, and the discrete velocity approximations will be denoted by $\mathbf{u}_i^{\text{SV}}$ resp. $\mathbf{u}_i^{\text{TH}}$ with $i = 1, \ldots, 5$. Since it is *a priori* unclear which discretization delivers better results, we will regard both $\mathbf{u}_5^{\text{SV}}$ and $\mathbf{u}_5^{\text{TH}}$ as reference solutions and we will then present the norm of the differences of all approximations against both reference solutions (Tables 7 and 8).

The values of this discrete L^2 error norm seem to be meaningful for the first, second and third levels of mesh refinement. The error $l^2_{961}(\mathbf{u}_5^{\text{SV}}, \mathbf{u}_5^{\text{TH}})$ between the two reference solutions is about 1.31×10^{-4}. On the first level, we observe that the l^2_{961} error of the Galerkin Taylor–Hood approximation is about 2.25 times larger

Table 7
Colliding flow (with symmetry assumption): convergence for Galerkin Scott–Vogelius approximations $\mathbf{u}_i^{\text{SV}}$ against the two reference solutions $\mathbf{u}_5^{\text{SV}}$ and $\mathbf{u}_5^{\text{TH}}$.

	$l^2_{961}(\mathbf{u}_1^{\text{SV}}, \cdot)$	$l^2_{961}(\mathbf{u}_2^{\text{SV}}, \cdot)$	$l^2_{961}(\mathbf{u}_3^{\text{SV}}, \cdot)$	$l^2_{961}(\mathbf{u}_4^{\text{SV}}, \cdot)$
$\mathbf{u}_5^{\text{SV}}$:	4.16201×10^{-3}	9.89292×10^{-4}	1.3798×10^{-4}	3.19216×10^{-5}
$\mathbf{u}_5^{\text{TH}}$:	4.16361×10^{-3}	9.97280×10^{-4}	1.90774×10^{-4}	1.35295×10^{-4}

Table 8
Colliding flow (with symmetry assumption): convergence for Galerkin Taylor–Hood approximations $\mathbf{u}_i^{\mathrm{TH}}$ against the two reference solutions $\mathbf{u}_5^{\mathrm{SV}}$ and $\mathbf{u}_5^{\mathrm{TH}}$.

	$l^2_{961}(\mathbf{u}_1^{\mathrm{TH}},\cdot)$	$l^2_{961}(\mathbf{u}_2^{\mathrm{TH}},\cdot)$	$l^2_{961}(\mathbf{u}_3^{\mathrm{TH}},\cdot)$	$l^2_{961}(\mathbf{u}_4^{\mathrm{TH}},\cdot)$
$\mathbf{u}_5^{\mathrm{SV}}$:	9.37985×10^{-3}	2.14044×10^{-3}	5.46704×10^{-4}	2.77048×10^{-4}
$\mathbf{u}_5^{\mathrm{TH}}$:	9.37439×10^{-3}	2.15659×10^{-3}	5.6353×10^{-4}	2.52655×10^{-4}

than the corresponding Scott–Vogelius error. For the second refinement level, we obtain a 2.14 times larger error for Taylor–Hood, and on the third level this factor grows to at least 2.86.

Therefore, we can definitely judge that in the given example of a colliding flow in a 2D cross-shaped domain at Reynolds number 1024 the Galerkin Scott–Vogelius element indeed yields slightly better results than the Galerkin Taylor–Hood element, provided the underlying mesh has adaptive mesh refinement at the boundary.

Finally, we demonstrate that indeed oscillations due to the term (18) are responsible for the better convergence behavior of the Galerkin Scott–Vogelius method. Therefore, we show the velocity approximations on the two lines

$$l_1 := \left\{\mathbf{x} = (x,0) : 0 \leqslant x \leqslant \frac{1}{2}\right\},$$
$$l_2 := \left\{\mathbf{x} = (x,0.4) : 0 \leqslant x \leqslant \frac{1}{2}\right\}$$

in Figs. 6 and 7.

The solution $(\mathbf{u}, p)$ in the physical domain Ω_{phys} is visualized in Fig. 8. In the center of the domain the flow field is at rest, corresponding to a maximum of the pressure. In the slip stream of the corners distinct vortices are visible.

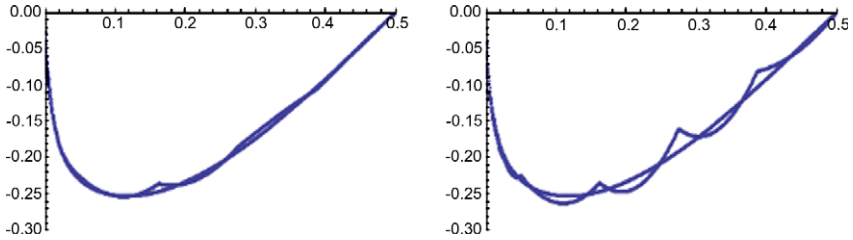

Fig. 6. Colliding flow (with symmetry assumption): different approximations for horizontal velocity component on line l_1. Reference solution (both pictures): Galerkin Scott–Vogelius at refinement level 5. Left picture: Galerkin Scott–Vogelius at refinement level 2. Right picture: Galerkin Taylor–Hood at refinement level 2.

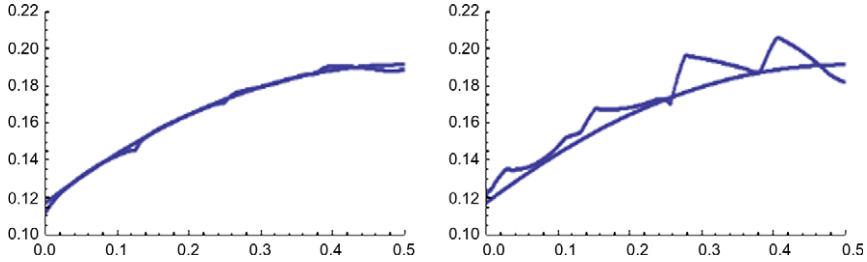

Fig. 7. Colliding flow (with symmetry assumption): different approximations for vertical velocity component on line l_2. Reference solution (both pictures): Galerkin Scott–Vogelius at refinement level 5. Left picture: Galerkin Scott–Vogelius at refinement level 2. Right picture: Galerkin Taylor–Hood at refinement level 2.

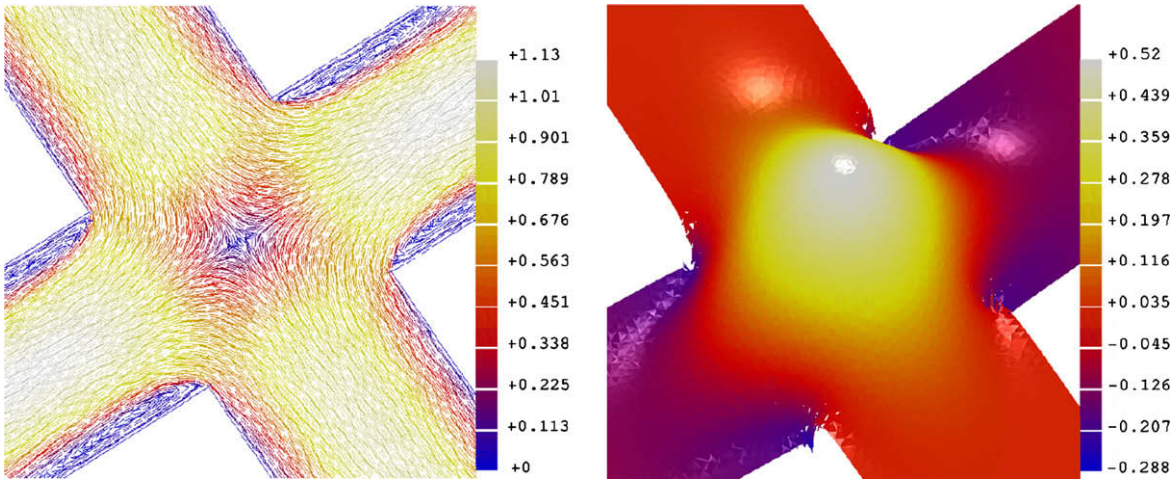

Fig. 8. Colliding flow example on the physical domain, i.e., without symmetry assumption: Left picture: flow field **u**. Color indicates the absolute values of the velocity. Right picture: pressure p. (For interpretation of the references to colour in this figure legend, the reader is referred to the web version of this article.)

7. Conclusion

Poor mass conservation in mixed finite element methods for incompressible flow problems can be a source of serious numerical instabilities. At large Reynolds numbers Re, numerical errors due to weak mass conservation are amplified by a factor Re. When force vectors with a large rotation-free part occur, the issue is most prominent, as it often appears in coupled flow problems. But the above steady 2d Navier–Stokes flow problem demonstrates, that poor mass conservation can also arise in uncoupled flow problems, where no force vector is prescribed. In such cases, the discrete convection term $(\mathbf{u}^h \cdot \nabla)\mathbf{u}^h$ possesses a rotation-free part and spoils the numerical computations. Especially concerning the discretization of the Oseen and Navier–Stokes equations it should be emphasized that the convection term is usually the source of two completely different numerical instabilities. Therefore, one should be careful in the explanation of spurious velocity oscillations in numerical computations for these problems. They can derive either from dominant convection or poor mass conservation, or even from a superposition of both effects. In order to separate both effects, we have used the divergence-free Scott–Vogelius element, and we have resolved possible boundary layers by the grid. The proposed flow problem can serve as a test example, in order to study, whether numerical discretizations of the incompressible Navier–Stokes equations possess a sufficient discrete mass conservation, and it has the advantage that it seems to be possible to generate similar real-world flows by physical experiments.

References

[1] H.W. Alt, Lineare Funktionalanalysis, Springer, Berlin, 1999.
[2] D.N. Arnold, J. Qin, Quadratic velocity/linear pressure Stokes elements, in: R. Vichnevetsky, D. Knight, G. Richter (Eds.), Advances in Computer Methods for Partial Differential Equations VII, IMACS, 1992, pp. 28–34.
[3] M. Braack, E. Burman, V. John, G. Lube, Stabilized finite element methods for the generalized Oseen problem, Comput. Methods Appl. Mech. Engrg. 196 (2007) 853–866.
[4] F. Brezzi, M. Fortin, Mixed and Hybrid Finite Elements, Springer, 1991.
[5] E. Burman, P. Hansbo, Edge stabilization for Galerkin approximations of convection–diffusion–reaction problems, Comput. Methods Appl. Mech. Engrg. 193 (2004) 1437–1453.
[6] E. Burman, A. Linke, Stabilized finite element schemes for incompressible flows using Scott–Vogelius elements, Appl. Numer. Math. 58 (2008) 1704–1719.
[7] R. Codina, Stabilized finite element approximation of transient incompressible flows using orthogonal subscales, Comput. Methods Appl. Mech. Engrg. 191 (2002) 4295–4321.
[8] A. Ern, J.L. Guermond, Theory and Practice of Finite Elements, Springer-Verlag, New York, 2004.
[9] S. Ganesan, V. John, Pressure separation – a technique for improving the velocity error in finite element discretisations of the Navier–Stokes equations, Appl. Math. Comput. 165 (2005) 275–290.
[10] K. Gärtner, O. Schenk, Solving unsymmetric sparse systems of linear equations with pardiso, in: Computational Science – ICCS 2002, Part II, Lecture Notes in Computational Science , ICCS, Berlin, 2002, pp. 355–363.
[11] T. Gelhard, G. Lube, M.A. Olshanskii, J.-H. Starcke, Stabilized finite element schemes with LBB-stable elements for incompressible flows, J. Comput. Appl. Math. 177 (2005) 243–267.
[12] V. Girault, P.-A. Raviart, Finite Element Methods for the Navier–Stokes Equations, Springer-Verlag, Berlin, 1986.
[13] D.F. Griffiths, The effect of pressure approximations on finite element calculations of incompressible flows, in: K.W. Morton, M.J. Baines (Eds.), Numerical Methods for Fluid Dynamics, Academic Press, London, 1982.
[14] V. John, S. Kaya, A finite element variational multiscale method for the Navier–Stokes equations, SIAM J. Sci. Comput. 26 (2005) 1485–1503.
[15] V. John, P. Knobloch, On spurious oscillations at layers diminishing (SOLD) methods for convection–diffusion equations: part I – a review, Comp. Meth. Appl. Mech. Engrg. 196 (2007) 2197–2215.
[16] V. John, P. Knobloch, On the performance of SOLD methods for convection–diffusion problems with interior layers, Int. J. Comp. Sci. Math. 1 (2007) 245–258.
[17] C. Johnson, J. Saranen, Streamline diffusion methods for the incompressible Euler and Navier–Stokes equations, Math. Comp. 47 (1986) 1–18.
[18] D. Kuzmin, On the design of algebraic flux correction schemes for quadratic finite elements, J. Comput. Appl. Math. 218 (2008) 79–87.
[19] A. Linke, Divergence-free mixed finite elements for the incompressible Navier–Stokes equation, Ph.D. Dissertation, University of Erlangen, 2007.
[20] A. Linke, G. Matthies, L. Tobiska, Non-nested multi-grid solvers for mixed divergence-free Scott–Vogelius discretizations, Computing 83 (2008) 87–107.
[21] G. Matthies, G. Lube, L. Röhe, Some remarks on streamline-diffusion methods for inf-sup stable discretisations of the generalised Oseen problem, Comp. Meths. Appl. Sc. (2009), accepted for publication.
[22] G. Matthies, P. Skrzypcz, L. Tobiska, A unified convergence analysis for local projection stabilisations applied to the Oseen problem, Math. Model. Numer. Anal. 41 (2007) 713–742.
[23] U. Nävert, A finite element method for convection–diffusion problems, Ph.D. Dissertation, Chalmers University of Technology, 1982.
[24] M.A. Olshanskii, A. Reusken, Grad-div stabilization for Stokes equations, Math. Comp. 73 (2004) 1699–1718.
[25] J. Qin, On the convergence of some low order mixed finite elements for incompressible fluids, Ph.D. Dissertation, Pennsylvania State University, 1994.
[26] H.-G. Roos, M. Stynes, L. Tobiska, Robust Numerical Methods for Singularly Perturbed Differential Equations, Convection–Diffusion–Reaction and Flow Problems, Springer, Berlin, 2008.
[27] M. Růžička, Nichtlineare Funktionalanalysis, Eine Einführung, Springer, 2004.
[28] F. Schieweck, Parallele Lösung der stationären inkompressiblen Navier–Stokes Gleichungen, Habilitation Thesis, University of Magdeburg, 1997.
[29] A. Schmidt, K.G. Siebert, Design of adaptive finite element software – the finite element toolbox ALBERTA, Lecture Notes in Computational Science and Engineering, vol. 42, Springer-Verlag, Berlin, 2005.
[30] L.R. Scott, M. Vogelius, Conforming finite element methods for incompressible and nearly incompressible continua, in: Large-Scale Computations in Fluid Mechanics, Part 2 Lectures in Applied Mathematics, vol. 22-2, 1985, pp. 221–244.
[31] J. Shewchuk, Triangle: a two-dimensional quality mesh generator and Delaunay triangulator, <http://www.cs.cmu.edu/quake/triangle.html>, University of California at Berkeley.
[32] M. Vogelius, An analysis of the *p*-version of the finite element method for nearly incompressible materials Uniformly valid optimal error estimates, Numer. Math. 41 (1983) 39–53.
[33] M. Vogelius, A right-inverse for the divergence operator in spaces of piecewise polynomials Application to the *p*-version of the finite element method, Numer. Math. 41 (1983) 19–37.